Eur. Phys. J. C 54, 187–197 (2008)
DOI 10.1140/epjc/s10052-007-0512-3

THE EUROPEAN PHYSICAL JOURNAL C

Regular Article – Theoretical Physics

Electroweak radiative corrections to the three channels of the process $f_1\bar{f}_1 ZA \to 0$

D. Bardin[1,a], S. Bondarenko[1,2,b], L. Kalinovskaya[1], G. Nanava[3,c], L. Rumyantsev[1], W. von Schlippe[4]

[1] Dzhelepov Laboratory for Nuclear Problems, JINR, Dubna, 141980, Russia
[2] Bogoliubov Laboratory of Theoretical Physics, JINR, Dubna, 141980, Russia
[3] IFJ, PAN, 31-342 Kraków, Poland
[4] PNPI, RAN, Gatchina, 188300, Russia

Received: 19 October 2007 / Revised version: 26 November 2007 /
Published online: 12 January 2008 –

Abstract. We have calculated the electroweak radiative corrections at the $\mathcal{O}(\alpha)$ level to the three channels of the process $f_1\bar{f}_1 ZA \to 0$ and implemented them into the SANC system. Here A stands for the photon and f_1 for a first generation fermion whose mass is neglected everywhere except in the arguments of logarithmic functions. The symbol $\to 0$ means that 4-momenta of all the external particles flow inwards. We present the complete analytical results for the covariant and helicity amplitudes for three cross channels: $f_1\bar{f}_1 \to Z\gamma$, $Z \to f_1\bar{f}_1\gamma$ and $f_1\gamma \to f_1 Z$. The one-loop scalar form factors of these channels are simply related by an appropriate permutation of their arguments, s, t, u. To check the correctness of our results we first of all observe the independence of the scalar form factors on the gauge parameters and the validity of the Ward identity, i.e. external photon transversality, and, secondly, compare our numerical results with the other independent calculations available to us.

PACS. 12.15.-y; 12.15.Lk

1 Introduction

The group developing the network client-server system SANC (*Support of Analytic and Numerical calculations for experiments at Colliders*) actively continues to implement processes that are of interest for LHC and ILC physics. SANC is one of a few systems, including Feynarts [1–3] and Grace-loop [4], in which calculations of elementary particle interactions were done at the one-loop precision level. A detailed description of version V.1.00 SANC was presented in [5]. The SANC client may be downloaded from two SANC servers [6, 7].

In the recent papers [8, 9] we presented an extension of the SANC **Processes** tree in the neutral current $ffbb$ sector, comprising the version V.1.10. In this paper we realize its further extension and include a calculation of the complete one-loop electroweak radiative corrections to the Z boson production channels $f_1\bar{f}_1 \to Z\gamma$ and $f_1\gamma \to f_1 Z$, and to the Z boson decay $Z \to f_1\bar{f}_1\gamma$. This class of processes was already mentioned in Sect. 2.7 of [5]. For this reason, we do not change the number of the SANC version; it is still V.1.10. The new processes are accessible from the $f_1 f_1 \to ZA$, $Z \to f_1 f_1 A$ and $f_1 A \to f_1 Z$ nodes, which are placed in the **Neutral Current** sector of the node **2f2b** on the electroweak part (**EW**) of the **Processes** tree; see Fig. 1. Each of these nodes contains standard modules of the scalar form factors (**FF**), helicity amplitudes (**HA**), and bremsstrahlung (**BR**).

The $Z\gamma$ production process is important for studies of the anomalous trilinear $Z\gamma\gamma$ and $ZZ\gamma$ gauge-boson couplings at the Fermilab tevatron [10–12], LHC [13, 14] and at the linear collider [15, 16] in both the e^+e^- and $e\gamma$ modes. The standard model (SM) of the electroweak interactions predicts no trilinear gauge coupling of the Z boson to the photon at the tree level. Any deviation of the couplings from the expected values would indicate the existence of new physics beyond the SM. At the LHC, one expects to observe hundreds of thousands of events of vector boson pair production. To match the precision of the LHC experiments, the vector boson pair production processes have to be considered beyond leading order [17].

Leptonic final states of the Z boson decays exhibit a very clear experimental signature and pave the way for precision tests of the SM beyond the leading order and for the possible detection of new physics. That is why it is necessary to fully control higher order EW corrections to the fermionic decays of the Z boson.

These processes were considered in the literature previously mostly in connection with their sensitivity to

[a] e-mail: bardin@nusun.jinr.ru
[b] e-mail: bondarenko@jinr.ru
[c] On leave from IHEP, TSU, Tbilisi, Georgia.

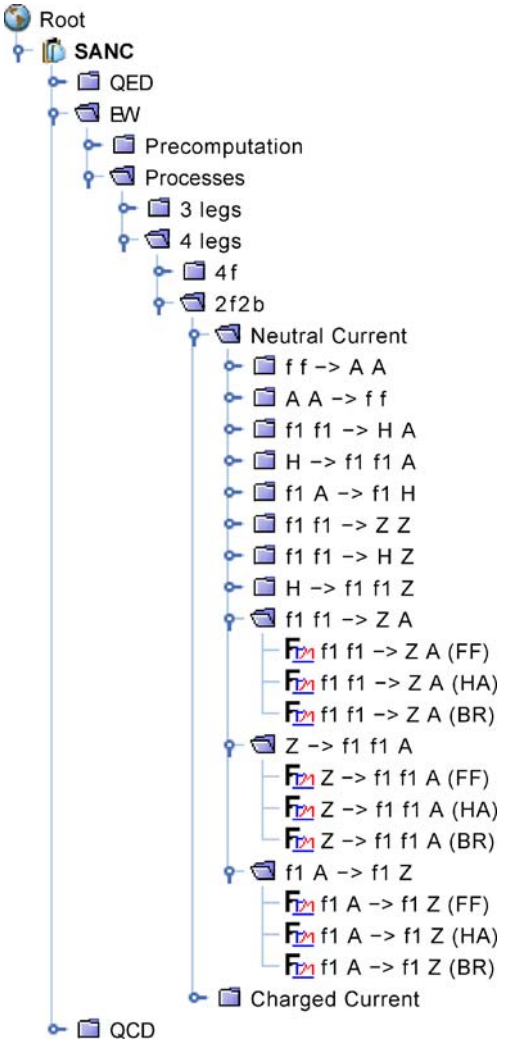

Fig. 1. New processes in the $ffbb$ sector

anomalous triple gauge couplings; see for example [18–21]. To our knowledge, the QED and EW corrections to Z boson production have been calculated previously only in [22–27]. The last paper contains results of calculations at the hadronic level that are beyond the scope of this paper. Not all of the first five papers could be used for a more or less tuned comparison. Below we show the comparison of numerical results with two papers: [24] and [26].

All the processes under consideration can be treated as various cross channels of the process $f_1\bar{f}_1Z\gamma \to 0$, and hence one-loop corrected scalar form factors, derived for this process, can be used for its cross channels also, after an appropriate permutation of their arguments (s,t,u). This is not the case for the helicity amplitudes, however. They are different for all three channels and must be calculated separately.

The paper is organized as follows. In Sect. 2 we demonstrate an analytic expression for the covariant amplitude at one-loop level in the annihilation channel. The helicity amplitudes for all three channels are given in Sect. 3. In Sect. 4 we present numerical results computed by FORTRAN codes generated with the s2n software and we consider a comparison with other independent calculations. Finally, summary remarks are given in Sect. 5.

2 Covariant amplitude

Let us consider the process

$$\bar{f}_1(p_1,\lambda_1)+f_1(p_2,\lambda_2)+\gamma(p_3,\lambda_3)+Z(p_4,\lambda_4)\to 0\,,$$

where the 4-momenta p_i $(i=1,2,3,4)$ of all external particles flow inwards. Here, the λ_i $(i=1,2,3,4)$ are the helicities of the corresponding particles. Schematically this process is given in Fig. 2, where the black blob represents the sum of all tree and one-loop self-energy, vertex and box type Feynman diagrams contributing to this process. Contributions of the counter term diagrams coming from the OMS renormalization procedure are assumed as well.

We found that next-to-leading order EW corrections to this process can be parametrized in terms of 28 scalar form factors (FF) and the corresponding basic matrix elements, 14 vector and 14 axial ones. For the covariant amplitude (CA) we have

$$\mathcal{A}_{\bar{f}_1f_1Z\gamma}=\bar{v}(p_1)\left[\mathrm{Str}^0_{\mu\nu}\left(v_f\mathcal{F}^0_{\mathrm{v}}+a_f\gamma_5\mathcal{F}^0_{\mathrm{a}}\right)+\sum_{j=1}^{13}\mathrm{Str}^j_{\mu\nu}\left(\mathcal{F}^j_{\mathrm{v}}+\gamma_5\mathcal{F}^j_{\mathrm{a}}\right)\right]u(p_2)\varepsilon^{\gamma}_{\nu}(p_3)\varepsilon^{Z}_{\mu}(p_4)\,, \tag{1}$$

with

$$\begin{aligned}
\mathrm{Str}^0_{\mu\nu}&=\mathrm{i}\left[\frac{1}{2}\left(\frac{1}{U^2+m_f^2}+\frac{1}{T^2+m_f^2}\right)\gamma_\mu\not{p}_3\gamma_\nu\right.\\
&\quad+\frac{1}{U^2+m_f^2}(\not{p}_3\delta_{\mu\nu}-\gamma_\nu(p_3)_\mu)\\
&\quad\left.-\left(\frac{p_{1\nu}}{U^2+m_f^2}-\frac{p_{2\nu}}{T^2+m_f^2}\right)\gamma_\mu\right], \qquad (2)\\
\mathrm{Str}^1_{\mu\nu}&=\mathrm{i}\gamma_\mu\not{p}_3\gamma_\nu\,,\\
\mathrm{Str}^2_{\mu\nu}&=\not{p}_3\gamma_\nu p_{1\mu}\,,\\
\mathrm{Str}^3_{\mu\nu}&=\not{p}_3\gamma_\nu p_{2\mu}\,,\\
\mathrm{Str}^4_{\mu\nu}&=\gamma_\mu\left[\not{p}_3p_{1\nu}-\frac{1}{2}\left(U^2+m_f^2\right)\gamma_\nu\right],\\
\mathrm{Str}^5_{\mu\nu}&=\gamma_\mu\left[\not{p}_3p_{2\nu}-\frac{1}{2}\left(T^2+m_f^2\right)\gamma_\nu\right],
\end{aligned}$$

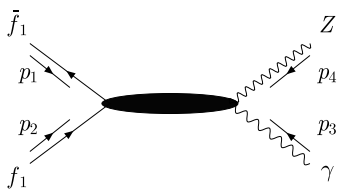

Fig. 2. The $\bar{f}_1f_1\gamma Z\to 0$ process

$$
\begin{aligned}
\mathrm{Str}^6_{\mu\nu} &= \mathrm{i}\left[\not{p}_3 p_{1\nu} - \frac{1}{2}\left(U^2+m_f^2\right)\gamma_\nu\right] p_{1\mu}\,,\\
\mathrm{Str}^7_{\mu\nu} &= \mathrm{i}\left[\not{p}_3 p_{2\nu} - \frac{1}{2}\left(T^2+m_f^2\right)\gamma_\nu\right] p_{1\mu}\,,\\
\mathrm{Str}^8_{\mu\nu} &= \mathrm{i}\left[\not{p}_3 p_{1\nu} - \frac{1}{2}\left(U^2+m_f^2\right)\gamma_\nu\right] p_{2\mu}\,,\\
\mathrm{Str}^9_{\mu\nu} &= \mathrm{i}\left[\not{p}_3 p_{2\nu} - \frac{1}{2}\left(T^2+m_f^2\right)\gamma_\nu\right] p_{2\mu}\,,\\
\mathrm{Str}^{10}_{\mu\nu} &= \mathrm{i}(\not{p}_3\delta_{\mu\nu} - \gamma_\nu (p_3)_\mu)\,,\\
\mathrm{Str}^{11}_{\mu\nu} &= \mathrm{i}\gamma_\mu\left[\left(T^2+m_f^2\right)p_{1\nu} - \left(U^2+m_f^2\right)p_{2\nu}\right]\,,\\
\mathrm{Str}_{12} &= p_{1\mu}p_{2\nu} + p_{2\mu}p_{2\nu} + \frac{1}{2}\left(T^2+m_f^2\right)\delta_{\mu\nu}\,,\\
\mathrm{Str}^{13}_{\mu\nu} &= \left[\left(T^2+m_f^2\right)p_{1\nu} - \left(U^2+m_f^2\right)p_{2\nu}\right]p_{2\mu}\,,
\end{aligned}
$$

where $\bar{v}(p_1)$, $u(p_2)$ and m_f are the bispinors and the mass of the external fermions, respectively; $\varepsilon^\gamma_\nu(p_3)$ denotes the photon polarization vector and $\varepsilon^Z_\mu(p_4)$ is the Z boson polarization vector; the vector and axial gauge-boson-to-fermion couplings are denoted by v_f and a_f, respectively; the $\mathcal{F}^j_{\mathrm{v,a}}$ are the scalar FF of the vector and axial vector currents, respectively; $\mathcal{F}^0_{\mathrm{v,a}}$ and $\mathrm{Str}^0_{\mu\nu}$ correspond to the lowest-order matrix elements. The usual Mandelstam invariants in Pauli metric ($p^2 = -m^2$) are defined as follows:

$$
\begin{aligned}
(p_1+p_2)^2 &= Q^2 = -s\,,\\
(p_2+p_3)^2 &= T^2 = -t\,,\\
(p_2+p_4)^2 &= U^2 = -u\,.
\end{aligned}
\tag{3}
$$

In (1) we keep the fermion mass in order to verify photon transversality for fully massive calculations, although a consistent treatment with massless fermions would also respect photon transversality, which, however, we do not use here in order to control the more general massive case.

The basic matrix elements, $\mathrm{Str}^j_{\mu\nu}$, are chosen to be explicitly transverse to the photonic 4-momentum. That is, for all of them the following relations hold:

$$
\mathrm{Str}^j_{\mu\nu}(p_3)_\nu \varepsilon^Z_\mu(p_4) = 0\,. \tag{4}
$$

Note the presence of the Z boson polarization vector $\varepsilon^Z_\mu(p_4)$, which is important to prove the Ward identity in a process with an on-mass-shell Z boson.

Then we neglect fermion masses where possible. However, in mass-containing denominators of $\mathrm{Str}^0_{\mu\nu}$, the mass cannot be neglected, because these denominators correspond to the propagators of fermions, which emit external photons and thus would lead to mass singularities.

We have checked that the FF $\mathcal{F}^j_{\mathrm{v,a}}$ are free of gauge parameters and of ultraviolet singularities (all calculations are done in the R_ξ gauge). The analytical expressions of the FF are too cumbersome to be presented in this paper. They can be reproduced on-line with the help of the SANC system. The CA for the processes we are interested in can be obtained from (1) exploiting crossing symmetry. This subject is covered in the next section.

3 Helicity amplitudes

In this section we collect the analytical expressions of the helicity amplitudes (HA) for all three channels. Let us briefly recall the SANC strategy of observable (cross section, differential distributions) calculations. In a first step, SANC constructs the CA of the process, free of gauge parameters and of ultraviolet singularities, taking into account all lowest-order and one-loop Feynman diagrams that contribute to the process. In the next step, the HA are calculated analytically and converted into numerical code. Further, the cross section or the decay width of the process is formed as the incoherent sum of squares of all possible HA:

$$
\mathrm{d}\sigma(\mathrm{d}\Gamma) \sim \sum_{\lambda_1\lambda_2\ldots\lambda_n} |\mathcal{H}_{\lambda_1\lambda_2\ldots\lambda_n}|^2\,\mathrm{d}\Phi^n\,, \tag{5}
$$

where squaring and summing is performed numerically. Finally, the Monte Carlo integrations over phase-space $\mathrm{d}\Phi^n$ are performed using the Vegas routine [28].

3.1 Annihilation channel $\bar{f}_1 f_1 \to Z\gamma$

To obtain the CA for the process

$$
\bar{f}_1(p_1,\lambda_1) + f_1(p_2,\lambda_2) \to \gamma(p_3,\lambda_3) + Z(p_4,\lambda_4)\,, \tag{6}
$$

where λ_i ($i = 1,2,3,4$) are the helicities of the external particles, we use the following substitutions of the 4-momenta in (1), see Fig. 3:

$$
\begin{aligned}
p_1 &\to p_1\,,\\
p_2 &\to p_2\,,\\
p_3 &\to -p_3\,,\\
p_4 &\to -p_4\,.
\end{aligned}
$$

The set of non-vanishing HA for this process, which we denote $\mathcal{H}_{\lambda_1\lambda_2\lambda_3\lambda_4}$, read

$$
\begin{aligned}
\mathcal{H}_{\mp\mp\mp\mp} = \frac{m_f}{\sqrt{s}}&\left[2 - \frac{1}{2}\frac{sZ_4(M_Z)}{Z_1(m_f)Z_2(m_f)}\sin^2\vartheta_\gamma\right] v_f \mathcal{F}_{v0}\\
&+ \frac{Z_4(M_Z)}{4\sqrt{s}} c_-\left[c_+(\mathcal{F}^\pm_2 - \mathcal{F}^\pm_3 - \mathcal{F}^\pm_4) - c_-\mathcal{F}^\pm_5\right.\\
&\left. + \mathcal{F}^\pm_{12} - \frac{s}{2}c_+\mathcal{F}^\pm_{13}\right]\,,
\end{aligned}
$$

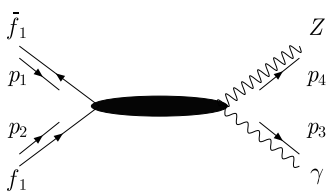

Fig. 3. Schematic representation of one-loop Feynman diagrams for the annihilation channel

$$
\begin{aligned}
\mathcal{H}_{\mp\mp\mp 0} &= \mp\frac{Z_4(M_Z)}{4\sqrt{2}M_Z}\sin\vartheta_\gamma\left[\frac{4M_Z^2 m_f}{Z_1(m_f)Z_2(m_f)}\cos\vartheta_\gamma v_f\mathcal{F}_{v0}\right.\\
&\quad + k_2\mathcal{F}_2^\pm + k_1\mathcal{F}_3^\pm - k_2\mathcal{F}_4^\pm + k_+c_-\mathcal{F}_5^\pm\\
&\quad \left. - s\mathcal{F}_{12}^\pm + \frac{s}{2}k_1\mathcal{F}_{13}^\pm\right],\\
\mathcal{H}_{\mp\mp\mp\pm} &= \frac{\sqrt{s}}{4}Z_4(M_Z)\sin^2\vartheta_\gamma\left[\frac{2m_f}{Z_1(m_f)Z_2(m_f)}v_f\mathcal{F}_{v0}\right.\\
&\quad \left. - \mathcal{F}_2^\pm + \mathcal{F}_3^\pm + \mathcal{F}_4^\pm - \mathcal{F}_5^\pm + \frac{s}{2}\mathcal{F}_{13}^\pm\right],\\
\mathcal{H}_{\mp\mp\pm\mp} &= \frac{\sqrt{s}}{8}Z_4(M_Z)\sin^2\vartheta_\gamma\\
&\quad \times\left[\frac{4m_f}{Z_1(m_f)Z_2(m_f)}v_f\mathcal{F}_{v0} + s\mathcal{F}_{13}^\pm\right],\\
\mathcal{H}_{\mp\mp\pm 0} &= \pm\frac{Z_4(M_Z)}{\sqrt{2}M_Z}\sin\vartheta_\gamma\left[\frac{m_f}{Z_1(m_f)Z_2(m_f)}\right.\\
&\quad \times\left(M_Z^2\cos\vartheta_\gamma v_f\mathcal{F}_{v0} \pm Z_4(M_Z)a_f\mathcal{F}_{a0}\right)\\
&\quad \left. - \frac{s}{4}\left(2\mathcal{F}_4^\pm + \mathcal{F}_{12}^\pm - \frac{1}{2}k_1\mathcal{F}_{13}^\pm\right)\right],\\
\mathcal{H}_{\mp\pm\pm\pm} &= \frac{m_f}{2\sqrt{s}}\left[\left(4 - \left(2Z_4(M_Z) + s\sin^2\vartheta_\gamma\right)\right.\right.\\
&\quad \left.\times\frac{Z_4(M_Z)}{Z_1(m_f)Z_2(m_f)}\right)v_f\mathcal{F}_{v0}\\
&\quad \left.\pm 2\frac{Z_4^2(M_Z)}{Z_1(m_f)Z_2(m_f)}\cos\vartheta_\gamma a_f\mathcal{F}_{a0}\right]\\
&\quad - \frac{\sqrt{s}}{2}Z_4(M_Z)\left(c_+\mathcal{F}_4^\pm - \frac{c_-}{2}\mathcal{F}_{12}^\pm + \frac{s}{4}\sin^2\vartheta_\gamma\mathcal{F}_{13}^\pm\right),\\
\mathcal{H}_{\pm\mp\pm\pm} &= \mp\frac{1}{8}\sin\vartheta_\gamma\left[\frac{4M_Z^2}{Z_1(m_f)}\mathcal{F}_0^\pm - Z_4(M_Z)\right.\\
&\quad \left.\times\left[sc_+(\mathcal{F}_6^\pm - \mathcal{F}_8^\pm) + 4\mathcal{F}_{10}^\pm + 2sc_-\mathcal{F}_{11}^\pm\right]\right],\\
\mathcal{H}_{\pm\mp\mp\mp} &= \pm\frac{1}{8}\sin\vartheta_\gamma\left[\frac{4M_Z^2}{Z_2(m_f)}\mathcal{F}_0^\pm - Z_4(M_Z)\right.\\
&\quad \left.\times\left[8\mathcal{F}_1^\pm + sc_-(\mathcal{F}_7^\pm - \mathcal{F}_9^\pm) - 4\mathcal{F}_{10}^\pm + 2sc_+\mathcal{F}_{11}^\pm\right]\right],\\
\mathcal{H}_{\pm\mp\pm 0} &= \frac{1}{8\sqrt{2}}\frac{\sqrt{s}}{M_Z}c_+\left[\frac{8M_Z^2}{Z_1(m_f)}\mathcal{F}_0^\pm + Z_4(M_Z)\right.\\
&\quad \left.\times\left(k_2\mathcal{F}_6^\pm + k_1\mathcal{F}_8^\pm - 4\mathcal{F}_{10}^\pm - 2k_+c_-\mathcal{F}_{11}^\pm\right)\right],\\
\mathcal{H}_{\mp\pm\pm 0} &= -\frac{1}{8\sqrt{2}}\frac{\sqrt{s}}{M_Z}c_-\left[\frac{8M_Z^2}{Z_2(m_f)}\mathcal{F}_0^\pm - Z_4(M_Z)\right.\\
&\quad \left.\times\left(8\mathcal{F}_1^\pm + k_2\mathcal{F}_7^\pm + k_1\mathcal{F}_9^\pm - 4\mathcal{F}_{10}^\pm + 2k_+c_+\mathcal{F}_{11}^\pm\right)\right],\\
\mathcal{H}_{\pm\mp\pm\mp} &= \mp\frac{s}{8}Z_4(M_Z)\sin\vartheta_\gamma c_+\left[\frac{2}{Z_1(m_f)Z_2(m_f)}\mathcal{F}_0^\pm\right.\\
&\quad \left. + \mathcal{F}_6^\pm - \mathcal{F}_8^\pm - 2\mathcal{F}_{11}^\pm\right],\\
\mathcal{H}_{\pm\mp\pm\pm} &= \pm\frac{s}{8}Z_4(M_Z)\sin\vartheta_\gamma c_-\left[\frac{2}{Z_1(m_f)Z_2(m_f)}\mathcal{F}_0^\pm\right.\\
&\quad \left. + \mathcal{F}_7^\pm - \mathcal{F}_9^\pm - 2\mathcal{F}_{11}^\pm\right], \qquad (7)
\end{aligned}
$$

with the following shorthand notation:

$$
\begin{aligned}
\mathcal{F}_0^\pm &= v_f\mathcal{F}_{v0}(s,t,u) \pm a_f\mathcal{F}_{a0}(s,t,u)\,,\\
\mathcal{F}_j^\pm &= \mathcal{F}_{vj}(s,t,u) \pm \mathcal{F}_{aj}(s,t,u)\,, \quad j = 1,\ldots,13,\\
k_{1,2} &= sc_\pm - M_Z^2 c_\mp\,, \quad c_\pm = 1 \pm \cos\vartheta_\gamma\,,\\
Z_1(m_f) &= \frac{1}{2}Z_4(M_Z)(1+\beta\cos\vartheta_\gamma)\,,\\
Z_2(m_f) &= \frac{1}{2}Z_4(M_Z)(1-\beta\cos\vartheta_\gamma)\,,\\
\beta &= \sqrt{1-4m_f^2/s}\,,\\
Z_4(M_Z) &= s - M_Z^2\,. \qquad (8)
\end{aligned}
$$

Here ϑ_γ is the center of mass system angle of the produced photon (angle between momenta $\mathbf{p}_2$ and $\mathbf{p}_3$), t and u are the Mandelstam variables

$$
t = m_f^2 - Z_2(m_f)\,, \quad u = m_f^2 - Z_1(m_f)\,. \qquad (9)
$$

3.2 Decay channel $Z \to f_1\bar{f}_1\gamma$

The CA of Z boson decay into fermion anti-fermion pairs and one real photon,

$$
Z(p_2,\lambda_2) \to \gamma(p_1,\lambda_1) + f_1(p_3,\lambda_3) + \bar{f}_1(p_4,\lambda_4)\,,
$$

is obtained by interchanging of 4-momenta in (1) as follows, see Fig. 4:

$$
\begin{aligned}
p_1 &\to -p_3\,,\\
p_2 &\to -p_4\,,\\
p_3 &\to -p_1\,,\\
p_4 &\to p_2\,.
\end{aligned}
$$

For the non-vanishing HA, $\mathcal{H}_{\lambda_2\lambda_1\lambda_3\lambda_4}$, we have

$$
\begin{aligned}
\mathcal{H}_{\pm\pm\pm\pm} &= -\frac{\sqrt{s}}{8}Z_2(M_Z)\sin^2\vartheta_f\\
&\quad \times\left[\frac{4m_f}{Z_3(m_f)Z_4(m_f)}v_f\mathcal{F}_{v0} + s\mathcal{F}_{13}^\pm\right],\\
\mathcal{H}_{\mp\mp\mp\pm} &= \mp\frac{s}{8}Z_2(M_Z)\sin\vartheta_f c_+\\
&\quad \times\left[\frac{2}{Z_3(m_f)Z_4(m_f)}\mathcal{F}_0^\pm + \mathcal{F}_7^\pm - \mathcal{F}_9^\pm - 2\mathcal{F}_{11}^\pm\right],
\end{aligned}
$$

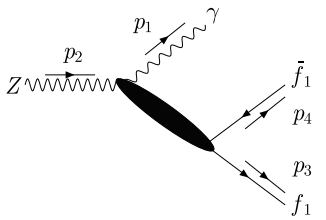

Fig. 4. Schematic representation of one-loop Feynman diagrams for the decay channel

$$
\begin{aligned}
\mathcal{H}_{\pm\pm\mp\pm} &= \pm\frac{s}{8} Z_2(M_Z)\sin\vartheta_f c_- \\
&\quad\times\left[\frac{2}{Z_3(m_f)Z_4(m_f)}\mathcal{F}_0^{\pm} + \mathcal{F}_6^{\pm} - \mathcal{F}_8^{\pm} - 2\mathcal{F}_{11}^{\pm}\right], \\
\mathcal{H}_{\mp\pm\mp\pm} &= \mp\frac{1}{8}\sin\vartheta_f\left[4\frac{M_Z^2}{Z_3(m_f)}\mathcal{F}_0^{\pm}\right. \\
&\quad\left. - Z_2(M_Z)(sc_-(\mathcal{F}_6^{\pm} - \mathcal{F}_8^{\pm}) + 4\mathcal{F}_{10}^{\pm} + 2sc_+\mathcal{F}_{11}^{\pm})\right], \\
\mathcal{H}_{\pm\mp\mp\pm} &= \pm\frac{1}{8}\sin\vartheta_f\left[4\frac{M_Z^2}{Z_4(m_f)}\mathcal{F}_0^{\pm} - Z_2(M_Z)\right. \\
&\quad\left.\times(8\mathcal{F}_1^{\pm} + sc_+(\mathcal{F}_7^{\pm} - \mathcal{F}_9^{\pm}) - 4\mathcal{F}_{10}^{\pm} + 2sc_-\mathcal{F}_{11}^{\pm})\right], \\
\mathcal{H}_{\mp\mp\pm\pm} &= -\frac{1}{8}\sqrt{s}Z_2(M_Z)\sin^2\vartheta_f\left[\frac{4m_f}{Z_3(m_f)Z_4(m_f)}v_f\mathcal{F}_{v0}\right. \\
&\quad\left. - 2(\mathcal{F}_2^{\pm} - \mathcal{F}_3^{\pm} - \mathcal{F}_4^{\pm} + \mathcal{F}_5^{\pm}) + s\mathcal{F}_{13}^{\pm}\right], \\
\mathcal{H}_{\pm\mp\pm\pm} &= -\frac{1}{4}\sqrt{s}\left[8\frac{m_f}{s}\frac{M_Z^2}{Z_2(M_Z)}v_f\mathcal{F}_{v0}\right. \\
&\quad - Z_2(M_Z)\left(\sin^2\vartheta_f(\mathcal{F}_2^{\pm} - \mathcal{F}_3^{\pm} - \mathcal{F}_4^{\pm})\right. \\
&\quad\left.\left. - c_+^2\mathcal{F}_5^{\pm} + c_+\mathcal{F}_{12}^{\pm} + \frac{s}{2}\sin^2\vartheta_f\mathcal{F}_{13}^{\pm}\right)\right], \\
\mathcal{H}_{\mp\pm\pm\pm} &= -\frac{1}{2}\sqrt{s}\left[4\frac{m_f}{s}\frac{M_Z^2}{Z_2(M_Z)}v_f\mathcal{F}_{v0}\right. \\
&\quad - 2\frac{m_f}{s}\frac{Z_2^2(M_Z)}{Z_3(m_f)Z_4(m_f)}(v_f\mathcal{F}_{v0} \pm \cos\vartheta_f a_f\mathcal{F}_{a0}) \\
&\quad\left. + Z_2(M_Z)\left(c_-\mathcal{F}_4^{\pm} - \frac{1}{2}c_+\mathcal{F}_{12}^{\pm} + \frac{s}{4}\sin^2\vartheta_f\mathcal{F}_{13}^{\pm}\right)\right], \\
\mathcal{H}_{0\pm\pm\pm} &= \frac{\mathrm{i}}{8\sqrt{2}}\frac{sZ_2(M_Z)}{M_Z}\sin\vartheta_f\left[\frac{8m_f}{sZ_3(m_f)Z_4(m_f)}\right. \\
&\quad\times\left(M_Z^2\cos\vartheta_f v_f\mathcal{F}_{v0} \pm Z_2(M_Z)a_f\mathcal{F}_{a0}\right) \\
&\quad\left. + 4\mathcal{F}_4^{\pm} + 2\mathcal{F}_{12}^{\pm} - k_2\mathcal{F}_{13}^{\pm}\right], \\
\mathcal{H}_{0\mp\pm\pm} &= \frac{\mathrm{i}}{4\sqrt{2}}\frac{Z_2(M_Z)}{M_Z}\sin\vartheta_f\left[\frac{4sm_f}{Z_3(m_f)Z_4(m_f)}\right. \\
&\quad\times\cos\vartheta_f v_f\mathcal{F}_{v0} - k_1\mathcal{F}_2^{\pm} - k_2\mathcal{F}_3^{\pm} + k_1\mathcal{F}_4^{\pm} \\
&\quad\left. - k_+c_+\mathcal{F}_5^{\pm} + s\mathcal{F}_{12}^{\pm} - \frac{s}{2}k_2\mathcal{F}_{13}^{\pm}\right], \\
\mathcal{H}_{0\mp\mp\pm} &= \mp\frac{\mathrm{i}}{\sqrt{2}}\frac{\sqrt{s}}{M_Z}\left[2\frac{M_Z^2}{Z_2(M_Z)}\mathcal{F}_0^{\pm} - \frac{1}{8}Z_2(M_Z)c_+\right. \\
&\quad\left.\times(8\mathcal{F}_1^{\pm} + k_1\mathcal{F}_7^{\pm} + k_2\mathcal{F}_9^{\pm} - 4\mathcal{F}_{10}^{\pm} + 2k_+c_-\mathcal{F}_{11}^{\pm})\right], \\
\mathcal{H}_{0\pm\mp\pm} &= \mp\frac{\mathrm{i}}{8\sqrt{2}}\frac{\sqrt{s}}{M_Z}\left[2\frac{M_Z^2}{Z_2(M_Z)}\mathcal{F}_0^{\pm} + \frac{1}{8}Z_2(M_Z)c_-\right. \\
&\quad\left.\times(k_1\mathcal{F}_6^{\pm} + k_2\mathcal{F}_8^{\pm} - 4\mathcal{F}_{10}^{\pm} - 2k_+c_+\mathcal{F}_{11}^{\pm})\right], \qquad (10)
\end{aligned}
$$

where $\mathcal{F}_j^{\pm}$ and the coefficients $k_{1,2}$ are defined by (8) and (9) with $c_\pm = 1 \pm \cos\vartheta_f$, and

$$
\begin{aligned}
Z_3(m_f) &= \frac{1}{2}Z_2(M_Z)(1 + \beta\cos\vartheta_f), \\
Z_4(m_f) &= \frac{1}{2}Z_2(M_Z)(1 - \beta\cos\vartheta_f), \\
s &= M_{f\bar{f}}^2, \quad t = m_f^2 + Z_4(m_f), \\
u &= m_f^2 + Z_3(m_f). \qquad (11)
\end{aligned}
$$

Here $Z_2(M_Z) = M_Z^2 - s$ and ϑ_f is the angle between the vector $\mathbf{p}_3$ and the direction defined by the photon momentum $\mathbf{p}_1$ in the rest frame of the system $(\mathbf{p}_3, \mathbf{p}_4)$. The photon momentum, $\mathbf{p}_1$, is chosen to be the direction of the z-axis in the $(\mathbf{p}_3, \mathbf{p}_4)$ rest frame.

3.3 Z production channel $e\gamma \to eZ$

Finally, in order to obtain the CA for the Z boson production channel

$$
\gamma(p_1, \lambda_1) + e^{\pm}(p_2, \lambda_2) \to e^{\pm}(p_3, \lambda_3) + Z(p_4, \lambda_4) \qquad (12)
$$

from (1), the 4-momenta permutations must be chosen as follows, see Fig. 5:

$$
\begin{aligned}
p_1 &\to -p_3, \\
p_2 &\to -p_4, \\
p_3 &\to -p_1, \\
p_4 &\to p_2.
\end{aligned}
$$

The HA, $\mathcal{H}_{\lambda_1\lambda_2\lambda_3\lambda_4}$, for this channel read

$$
\begin{aligned}
\mathcal{H}_{\pm\mp\mp\pm} &= \frac{k_3}{\sqrt{2s}}\left[2\left(\frac{1}{k_-} - \frac{1}{Z_3(m_e)}\right)M_Z^2\mathcal{F}_0^{\pm}\right. \\
&\quad\left. + sc_-\left(\frac{k_-}{4}c_+\mathcal{F}_8^{\pm} - \mathcal{F}_{10}^{\pm} + k_-\mathcal{F}_{11}^{\pm}\right)\right], \\
\mathcal{H}_{\pm\mp\mp0} &= \pm\frac{k_4}{M_Z}\left[\frac{2M_Z^2}{k_-}\mathcal{F}_0^{\pm} + \frac{1}{2}c_+\left(\frac{k_-^2}{2}\mathcal{F}_6^{\pm} - \frac{k_-}{4}k_1\mathcal{F}_8^{\pm}\right.\right. \\
&\quad\left.\left. + k_+\mathcal{F}_{10}^{\pm} - sk_-\mathcal{F}_{11}^{\pm}\right)\right],
\end{aligned}
$$

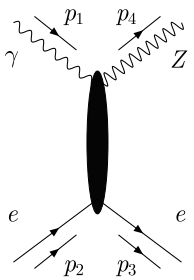

Fig. 5. Schematic representation of one-loop Feynman diagrams for the Z boson production channel

$$
\begin{aligned}
\mathcal{H}_{\pm\mp\pm 0} &= \frac{k_3}{M_Z\sqrt{s}}\left[\frac{2m_e}{Z_3(m_e)}\right.\\
&\quad\times\left(M_Z^2\left(\frac{s}{k_-}+1\right)v_e\mathcal{F}_{v_0}\pm\frac{s^2}{k_-}a_e\mathcal{F}_{a_0}\right)\\
&\quad\left.+\frac{s}{4}c_-\left(2k_-\mathcal{F}_4^{\pm}+k_+\mathcal{F}_{12}^{\pm}-\frac{k_-}{2}k_1\mathcal{F}_{13}^{\pm}\right)\right],\\
\mathcal{H}_{\pm\mp\pm\pm} &= \mp\frac{k_4}{\sqrt{2}}\left[\frac{2sm_e}{Z_3(m_e)k_-}\mathcal{F}_{v_0}^{\pm}\right.\\
&\quad\left.+\frac{s}{2}c_-\left(\mathcal{F}_{12}^{\pm}-\frac{k_-}{2}c_+\mathcal{F}_{13}^{\pm}\right)\right],\\
\mathcal{H}_{\pm\mp\pm\mp} &= \mp\frac{k_4}{\sqrt{2}}c_+\left[k_-\mathcal{F}_4^{\pm}+\frac{s}{2}\left(\mathcal{F}_{12}^{\pm}+\frac{k_-}{2}c_-\mathcal{F}_{13}^{\pm}\right)\right],\\
\mathcal{H}_{\mp\mp\pm 0} &= -\frac{\sqrt{s}k_3}{M_Z}\left[\frac{2M_Z^2m_e}{sZ_3(m_e)}v_e\mathcal{F}_{v_0}-k_-\mathcal{F}_2^{\pm}+\frac{1}{2}k_1\mathcal{F}_3^{\pm}\right.\\
&\quad\left.+k_-\mathcal{F}_4^{\pm}-s\mathcal{F}_5^{\pm}+\frac{1}{4}c_-\left(k_+\mathcal{F}_{12}^{\pm}-\frac{k_-}{2}k_1\mathcal{F}_{13}^{\pm}\right)\right],\\
\mathcal{H}_{\mp\mp\mp\mp} &= \left(\frac{s}{2}\right)^{\frac{3}{2}}k_3c_-\mathcal{F}_9^{\pm},\\
\mathcal{H}_{\mp\mp\pm 0} &= \pm\frac{sk_4}{M_Z}\left[2\mathcal{F}_1^{\pm}-\frac{k_-}{2}\mathcal{F}_7^{\pm}+\frac{1}{4}k_1\mathcal{F}_9^{\pm}\right.\\
&\quad\left.-\mathcal{F}_{10}^{\pm}+\frac{k_-}{2}c_+\mathcal{F}_{11}^{\pm}\right],\\
\mathcal{H}_{\mp\mp\pm\pm} &= -\frac{k_3}{\sqrt{2s}}\left[\frac{2k_-}{Z_3(m_e)}\mathcal{F}_0^{\pm}\right.\\
&\quad\left.-s\left(4\mathcal{F}_1^{\pm}-\frac{s}{2}c_-\mathcal{F}_9^{\pm}-2\mathcal{F}_{10}^{\pm}-k_-c_-\mathcal{F}_{11}^{\pm}\right)\right],\\
\mathcal{H}_{\mp\mp\pm\mp} &= \mp\frac{sk_4}{\sqrt{2}}\left[c_+\mathcal{F}_3^{\pm}-2\mathcal{F}_5^{\pm}+\frac{1}{2}c_-\left(\mathcal{F}_{12}^{\pm}-\frac{k_-}{2}c_+\mathcal{F}_{13}^{\pm}\right)\right],\\
\mathcal{H}_{\mp\mp\pm\pm} &= \pm\frac{sk_4}{\sqrt{2}}c_+\left[\mathcal{F}_3^{\pm}-\frac{1}{2}\mathcal{F}_{12}^{\pm}-\frac{k_-}{4}c_-\mathcal{F}_{13}^{\pm}\right],\\
\mathcal{H}_{\pm\mp\mp\mp} &= -\sqrt{\frac{s}{2}}k_3\left[\frac{2}{k_-}\mathcal{F}_0^{\pm}+c_+\left(\frac{k_-}{4}c_-\mathcal{F}_8^{\pm}+\mathcal{F}_{10}^{\pm}\right)\right].
\end{aligned}
\tag{13}
$$

Here the coefficients $k_{3,4,\pm}$ are defined by

$$
\begin{aligned}
&k_3 = N_-\cos\frac{\vartheta_e}{2}, \quad k_4 = N_-\sin\frac{\vartheta_e}{2},\\
&k_\pm = s\pm M_Z^2,
\end{aligned}
\tag{14}
$$

with

$$
N_- = \sqrt{\frac{s-M_Z^2}{2}}, \tag{15}
$$

$Z_2(m_e)$ and $Z_3(m_e)$ are the denominators of the fermionic propagators:

$$
\begin{aligned}
Z_2(m_e) &= s-m_e^2,\\
Z_3(m_e) &= \frac{Z_2(m_e)}{2s}\Big[s+m_e^2-M_Z^2\\
&\quad+\sqrt{\lambda\big(s,m_e^2,M_Z^2\big)}\cos\vartheta_e\Big],
\end{aligned}
\tag{16}
$$

ϑ_e denotes the $e^{\pm}$ scattering angle and $\lambda(s,m_e^2,M_Z^2)$ is the kinematical Källen function.

The Mandelstam variables transform as follows:

$$
\begin{aligned}
s &\to -\frac{1}{2}\left[\left(s-\frac{M_Z^2m_e^2}{s}-M_Z^2-2m_e^2+\frac{m_e^4}{s}\right)\right.\\
&\quad\left.-\frac{s-m_e^2}{s}\sqrt{\lambda\big(s,m_e^2,M_Z^2\big)}\cos\vartheta_e\right],\\
u &\to -\frac{1}{2}\left[\left(s+\frac{M_Z^2m_e^2}{s}-M_Z^2-2m_e^2-\frac{m_e^4}{s}\right)\right.\\
&\quad\left.+\frac{s-m_e^2}{s}\sqrt{\lambda\big(s,m_e^2,M_Z^2\big)}\cos\vartheta_e\right],\\
t &\to s\,.
\end{aligned}
$$

4 Numerical results and comparison

In this section we present the SANC predictions for various observables of all three processes under consideration. The tree level and single real photon emission contributions are compared with CompHEP, while one-loop electroweak and QED corrections for the production channel $e\gamma \to eZ$ are checked against the Grace-loop package [4] and [26]. Note that all numerical results of this section are produced with the standard SANC INPUT (Sect. 6.2.3 of [9]) if not stated otherwise.

4.1 Annihilation channel $\bar{f}_1 f_1 \to Z\gamma$

For the process $\bar{f}_1 f_1 \to Z\gamma$ we show in Table 1 a comparison between SANC and CompHEP results for the Born level cross sections computed without any cuts, and the cross sections of hard photon radiation computed with a cut on the photon energies, chosen to be equal for processes with two identical photons in the final state.

As can be seen from Table 1, we found very good agreement for the Born cross section. For the hard contribution we have perfect agreement at $\sqrt{s} = 100\,\text{GeV}$, then a difference rapidly rising with energy, and eventually unstable CompHEP predictions for $\sqrt{s}$ at and above 1 TeV.

As seen from Table 2 for the process $\mu^+\mu^- \to Z\gamma(\gamma)$, the hard contributions stay closer (though statistically are

Table 1. Comparison of the Born and hard cross sections of the $e^+e^- \to Z\gamma(\gamma)$ process; SANC first rows, CompHEP second rows. (CompHEP input, $E_\gamma \geq 1\,\text{GeV}$). The uncertainty of the last significant digit is given in brackets

	σ [pb]			
$\sqrt{s}$ [GeV]	100	200	500	1000
Born	2482(0)	86.23(0)	11.65(0)	2.985(0)
Born	2482(0)	86.23(0)	11.65(0)	2.985(0)
Hard	586.7(7)	43.26(8)	7.69(2)	2.341(6)
Hard	586.7(3)	42.48(5)	7.47(1)	unstable

Table 2. The same as Table 1 but for the process $\mu^+\mu^- \to Z\gamma(\gamma)$

	σ [pb]			
$\sqrt{s}$ [GeV]	100	200	500	1000
Born	1349(0)	49.09(0)	6.979(0)	1.847(0)
Born	1349(0)	49.09(0)	6.979(0)	1.847(0)
Hard	173.8(0)	14.14(0)	2.798(1)	0.923(0)
Hard	173.8(0)	14.08(2)	2.763(2)	0.905(1)

Table 3. The same as Table 1 but for the process $\tau^+\tau^- \to Z\gamma(\gamma)$

	σ [pb]			
$\sqrt{s}$ [GeV]	100	200	500	1000
Born	749.2(0)	29.43(0)	4.508(0)	1.246(1)
Born	749.2(0)	29.43(0)	4.508(0)	1.246(1)
Hard	53.56(1)	5.073(2)	1.170(1)	0.421(1)
Hard	53.56(1)	5.072(1)	1.169(1)	0.417(1)

incompatible) within a wider range of $\sqrt{s}$. This is even more pronounced for the non-existing process $\tau^+\tau^- \to Z\gamma(\gamma)$; the figures, shown in Table 3, agree well within statistical errors. This tendency points to the origin of the difference being due to collinear singularities of the integrand.

The stability against variation of $\bar{\omega}$ discussed below gives us a great level of confidence in the SANC results.

In Tables 4–6 we present the results of our calculations for the annihilation channels $e^+e^- \to Z\gamma(\gamma)$, $\bar{u}u \to Z\gamma(\gamma)$ and $\bar{d}d \to Z\gamma(\gamma)$, respectively, carried out with 10M statistics for the hard cross section for five energies and at each energy for two values of $\bar{\omega}$: $\bar{\omega} = 10^{-5}\sqrt{s}/2$ (subscript 1) and $10^{-6}\sqrt{s}/2$ (subscript 2); for the σ in pb and for $\delta = \sigma^{\text{1-loop}}/\sigma^{\text{Born}} - 1$ in %.

The total one-loop cross section $\sigma^{\text{1-loop}}$ is the sum of the Born, virtual, soft and hard contributions:

$$\sigma^{\text{1-loop}} = \sigma^{\text{Born}} + \sigma^{\text{virt}}(\lambda) + \sigma^{\text{soft}}(\lambda, \bar{\omega}) + \sigma^{\text{hard}}(\bar{\omega}) .$$

Here σ^{virt} and σ^{soft} depend on the regularizing parameter λ, which cancels in their sum. This cancellation was checked on the algebraic level. The contributions σ^{soft} and σ^{hard} depend on $\bar{\omega}$, the soft/hard separation parameter.

This dependence must cancel on the numerical level. To ascertain this cancellation we have the calculation at each energy for two values of $\bar{\omega}$ as shown above. Comparing the corresponding values of $\sigma^{\text{1-loop}}$ and of δ, we can see that there is no change outside the statistical errors of the Monte Carlo integration.

The following cuts were imposed:

- CMS angular cuts for the Born, soft and virtual contributions where there is only one photon in the final state: $\vartheta_{\gamma,\,Z} \in [1^\circ, 179^\circ]$;
- CMS angular cuts on the Z boson and on the two photons and CMS energy cuts on the photons for the hard contribution: for the event to be accepted, ϑ_Z and at least one of ϑ_{γ_1} or ϑ_{γ_2} must lie in the interval $[1^\circ, 179^\circ]$, and both photons must have a CMS energy greater than $\bar{\omega}$.

One should stress that these cuts are different from those used for Tables 1–3. Here we impose angular cuts that strongly affect the Born cross sections. As far as hard cross sections are concerned, we cut here at a small value of the soft–hard separator $\bar{\omega}$ in order to match

Table 4. Comparison of the Born and one-loop cross sections of the annihilation channel $e^+e^- \to Z\gamma(\gamma)$ calculated with different values of the soft–hard separation parameter $\bar{\omega}$; for details see the text

$\sqrt{s}$ [GeV]	200	500	1000	2000	5000
σ^{Born} [pb]	27.8548(1)	3.37334(1)	0.816485(2)	0.202534(1)	0.0323355(1)
$\sigma_1^{\text{1-loop}}$ [pb]	43.36(4)	5.216(9)	1.239(4)	0.299(1)	0.0436(3)
$\sigma_2^{\text{1-loop}}$ [pb]	43.38(5)	5.211(10)	1.235(4)	0.298(2)	0.0430(5)
δ_1 [%]	55.7(2)	54.6(3)	51.9(4)	47.4(6)	34.9(8)
δ_2 [%]	55.7(2)	54.5(3)	51.3(5)	46.9(8)	33.0(14)

Table 5. Comparison of the Born and one-loop cross sections of the annihilation channel $\bar{u}u \to Z\gamma(\gamma)$ calculated with different values of the soft–hard separation parameter $\bar{\omega}$

$\sqrt{s}$ [GeV]	200	500	1000	2000	5000
σ^{Born} [pb]	4.7504(1)	0.57540(0)	0.13927(0)	0.034548(0)	0.005516(0)
$\sigma_1^{\text{1-loop}}$ [pb]	5.3399(8)	0.6472(2)	0.15367(6)	0.036458(2)	0.005203(6)
$\sigma_2^{\text{1-loop}}$ [pb]	5.3392(9)	0.6470(2)	0.17159(7)	0.036458(2)	0.005193(7)
δ_1 [%]	12.41(2)	12.48(3)	10.34(4)	5.54(6)	−5.67(11)
δ_2 [%]	12.39(2)	12.44(3)	10.28(5)	5.53(8)	−5.84(12)

Table 6. Comparison of the Born and one-loop cross sections of the annihilation channel $\bar{d}d \to Z\gamma(\gamma)$ calculated with different values of the soft–hard separation parameter $\bar{\omega}$

$\sqrt{s}$ [GeV]	200	500	1000	2000	5000
σ^{Born} [pb]	1.5230(0)	0.18450(0)	0.044658(0)	0.011078(0)	0.0017686(0)
$\sigma_1^{\text{1-loop}}$ [pb]	1.6033(1)	0.18920(1)	0.043823(4)	0.009992(2)	0.0012825(4)
$\sigma_2^{\text{1-loop}}$ [pb]	1.6033(1)	0.18924(1)	0.043825(5)	0.009992(2)	0.0012826(4)
δ_1 [%]	5.274(4)	2.549(6)	−1.869(10)	−9.807(14)	−27.486(23)
δ_2 [%]	5.275(4)	2.570(7)	−1.865(11)	−9.804(16)	−27.479(27)

the hard contribution with the corresponding soft one. This is why the figures from these tables cannot be compared.

For all tables, the numbers in brackets give the statistical uncertainties of the last digit shown.

Finally, we tried to reproduce Fig. 8 of [27]. Our version of it is presented in Fig. 6.

Although we observe only qualitative agreement, we are more or less satisfied with it, because a tuned comparison is not possible due to lack of a complete list of input parameters in [27]. Later on, in Sect. 4.3 for the crossed channel, we realize a tuned comparison and find complete agreement. This gives us confidence in our result and we believe that, if we had a chance to make a tuned comparison here, we would reach a better agreement for the annihilation channel as well.

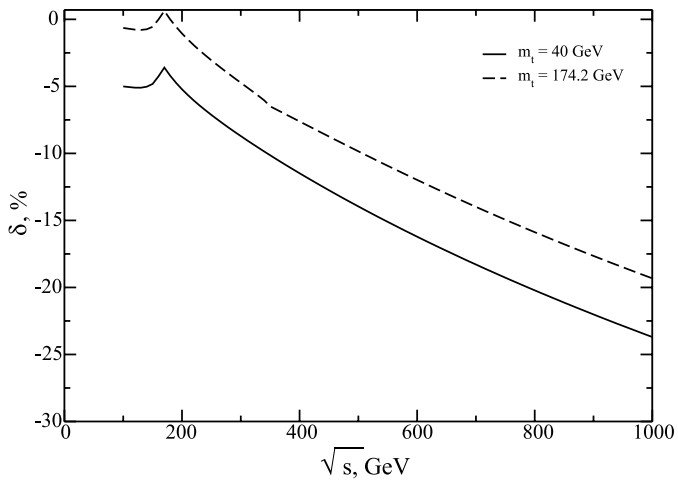

Fig. 6. Energy dependence of the total one-loop correction for 90° scattering

4.2 Decay channel $Z \to f_1\bar{f}_1\gamma$

In Table 7 we present the results of a comparison of the Born cross section and the cross section of hard photon bremsstrahlung of Z boson decay between SANC and CompHEP. We see that we have excellent agreement between these two programs. Differences are within statistical errors.

In Table 8 we show the differential decay rate $\mathrm{d}\Gamma/\mathrm{d}s \times 10^8$ in GeV^{-1} of the decay $Z \to \mu^+\mu^-\gamma(\gamma)$, where $\sqrt{s}$ is the invariant mass of the $\mu^+\mu^-$ pair calculated with two different values of the soft–hard separation parameter $\bar{\omega}$: 10^{-4} GeV (subscript 1) and 10^{-5} GeV (subscript 2). The quantity δ is given by $\delta = (\mathrm{d}\Gamma^{\text{1-loop}}/\mathrm{d}s - \mathrm{d}\Gamma^{\text{Born}}/\mathrm{d}s)/\mathrm{d}\Gamma^{\text{Born}}/\mathrm{d}s$.

In Fig. 7 we show the differential decay widths $\mathrm{d}\Gamma^{\text{Born}}/\mathrm{d}s$ and $\mathrm{d}\Gamma^{\text{1-loop}}/\mathrm{d}s$ for the decay $Z \to \mu^+\mu^-\gamma(\gamma)$ as functions of $\sqrt{s} = M_{\mu^+\mu^-}$.

Table 7. Comparison of the Born and hard widths of the $Z \to \mu^+\mu^-\gamma(\gamma)$ decay; SANC first rows, CompHEP second rows. (CompHEP input, $E_\gamma > \omega$ for photon(s)). The uncertainty of the last significant digit is given in brackets

	Γ [MeV]			
ω [GeV]	0.1	1	2	5
Born	27.730(1)	15.779(1)	12.269(1)	7.8271(1)
Born	27.730(1)	15.778(1)	12.269(1)	7.8268(1)
Hard	4.393(2)	1.358(1)	0.7944(4)	0.2941(2)
Hard	4.392(3)	1.359(1)	0.7940(5)	0.2946(2)

Table 8. Comparison of the Born and one-loop differential widths of the decay channel $Z \to \mu^+\mu^-\gamma(\gamma)$ calculated with different values of the soft–hard separation parameter $\bar{\omega}$; for details see the text

$\sqrt{s}$ [GeV]	1.	10.	20.	50.	70.
$\mathrm{d}\Gamma^{\text{Born}}/\mathrm{d}s$ [GeV^{-1}]	7.918	18.57	22.63	39.98	89.11
$\mathrm{d}\Gamma_1^{\text{1-loop}}/\mathrm{d}s$ [GeV^{-1}]	744.21(4)	18.834(4)	21.949(8)	35.92(2)	76.12(6)
$\mathrm{d}\Gamma_2^{\text{1-loop}}/\mathrm{d}s$ [GeV^{-1}]	744.21(4)	18.830(5)	21.937(10)	35.93(3)	76.16(8)
δ_1	92.992(5)	0.0140(2)	−0.0300(3)	−0.1014(6)	−0.1458(7)
δ_2	92.992(5)	0.0137(3)	−0.0305(4)	−0.1014(8)	−0.1452(9)

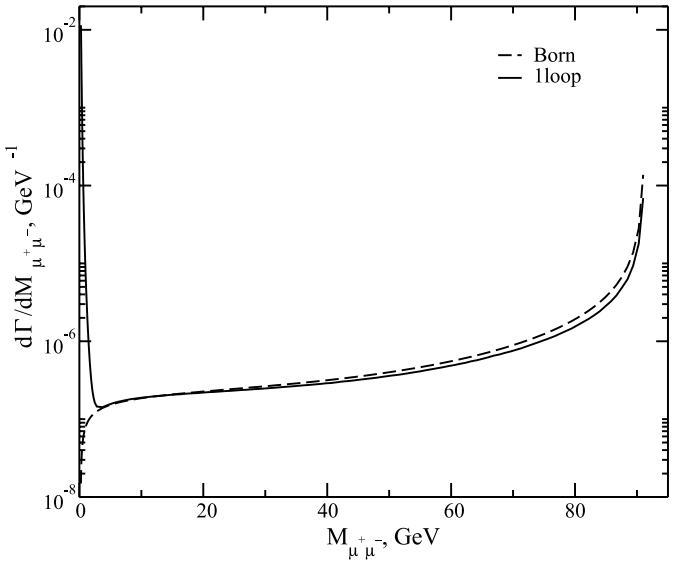

Fig. 7. Invariant mass distribution of the $\mu^+\mu^-$ pair for the decay $Z \to \mu^+\mu^-\gamma(\gamma)$. Both the Born (*dashed line*) and the one-loop (*dotted line*) results are shown

The Coulomb peak, which is due to photon exchange in the Feynman one-loop diagram with a $\gamma Z\gamma$ three-boson vertex, is clearly seen.

4.3 Z production channel $e\gamma \to eZ$

As can be seen from Table 9, we have again very good agreement between the SANC and CompHEP predictions for the tree level and real photon emission cross sections of this process.

In Table 10 we present the results of our calculations for the channel $\gamma e^- \to Ze^-(\gamma)$ carried out with 10M statistics for the hard cross section for five energies and at each energy for two values of $\bar{\omega}$: $\bar{\omega} = 10^{-5}\sqrt{s}/2$ (subscript 1) and $10^{-6}\sqrt{s}/2$ (subscript 2).

The notation of the various contributions, σ^{Born} etc., is as in the previous case.

The cancellation of the λ-dependent terms was again checked on the algebraic level. The cancellation of the $\bar{\omega}$ dependence on the numerical level was tested as in the previous case. Comparing the corresponding values of $\sigma^{\text{1-loop}}$ and of δ we can see again that there is no change outside the statistical errors of the Monte Carlo integration.

Table 9. Comparison of the Born cross sections for the $\gamma e^- \to Ze^-$ reaction and of the hard cross sections for the $\gamma\mu^- \to Z\mu^-\gamma$ reaction; SANC first rows, CompHEP second rows. (CompHEP input, $E_\gamma \geq 1$ GeV)

	σ [pb]			
$\sqrt{s}$ [GeV]	100	200	500	1000
Born	82.27(0)	23.72(0)	5.575(0)	1.534(0)
Born	82.27(0)	23.72(0)	5.575(0)	1.534(0)
Hard	4.012(1)	3.689(2)	1.368(1)	0.4986(6)
Hard	4.014(0)	3.688(1)	1.364(1)	0.4973(6)

The following cuts were imposed:

- CMS angular cuts for the Born cross section and for the contributions with Born-like kinematics: $\vartheta_{e,Z} \in [1^\circ, 179^\circ]$;
- CMS angular cuts on the Z boson and on the photon and a CMS energy cut on the electron for the hard contribution: for the event to be accepted, ϑ_Z and ϑ_e must lie in the interval $[1^\circ, 179^\circ]$, and the photon must have a CMS energy greater than $\bar{\omega}$.

The numbers in brackets give the statistical uncertainties of the last digit shown.

In Table 11 we show the comparison of the Born cross sections: the angular distributions $\mathrm{d}\sigma/\mathrm{d}\cos\vartheta_e$ and the cross sections integrated over the given angular intervals, as well as the one-loop EW corrections δ, produced by three programs: that of [26], Grace-loop [4] and SANC.

We have excellent agreement between these three results. Note that in this table the results taken from the literature were given there without statistical errors. The statistical errors of numbers obtained with SANC are in the digits beyond those shown.

5 Conclusions

In this paper we describe the implementation of the complete one-loop EW calculations, including hard bremsstrahlung contributions, for the process $f_1\bar{f}_1 ZA \to 0$ into the SANC framework. The calculations were done using a combination of analytic and Monte Carlo integration methods, which make it easy to calculate a variety of

Table 10. Comparison of the Born and one-loop cross sections of channel $\gamma e^- \to Ze^-(\gamma)$ calculated with different values of the soft–hard separation parameter $\bar{\omega}$

$\sqrt{s}$ [GeV]	200	500	1000	2000	5000
σ^{Born} [pb]	8.3381(3)	1.7917(0)	0.46840(0)	0.11842(0)	0.019007(0)
$\sigma_1^{\text{1-loop}}$ [pb]	8.7988(5)	1.9591(2)	0.52129(5)	0.13171(1)	0.02037(2)
$\sigma_2^{\text{1-loop}}$ [pb]	8.8002(9)	1.9593(2)	0.52131(6)	0.13168(1)	0.02037(3)
δ_1 [%]	5.54(1)	9.35(1)	11.29(1)	11.23(1)	7.16(1)
δ_2 [%]	5.54(1)	9.36(1)	11.30(1)	11.20(1)	7.15(2)

Table 11. Triple comparison of the Born cross section and of the correction $\delta = \sigma^{\text{1-loop}}/\sigma^{\text{Born}} - 1$ for channel $\gamma e^- \to Ze^-(\gamma)$ ([26] input, $E_\gamma = 0.025\sqrt{s}\,\text{GeV}$)

$\sqrt{s}$ [GeV]	ϑ		[26]	Grace-loop	SANC
	20°	σ^{Born} [pb]	0.3931		0.39308
		δ [%]	−5.96		−5.9556
	90°	σ^{Born} [pb]	0.6491		0.64906
		δ [%]	−8.56		−8.5562
100	160°	σ^{Born} [pb]	9.038		9.0383
		δ [%]	−10.00		−10.005
	$20^\circ < \theta < 160^\circ$	σ^{Born} [pb]	13.051		13.051
		δ [%]	−9.04		−9.0389
	$1^\circ < \theta < 179^\circ$	σ^{Born} [pb]	33.484		33.484
		δ [%]	−10.27		−10.273
	20°	σ^{Born} [pb]	0.02898		0.028984
		δ [%]	−30.08		−30.079
	90°	σ^{Born} [pb]	0.03598		0.035985
		δ [%]	−26.74		−26.744
500	160°	σ^{Born} [pb]	0.4661		0.46607
		δ [%]	−23.05		−23.054
	$20^\circ < \theta < 160^\circ$	σ^{Born} [pb]	0.7051	0.70515	0.70515
		δ [%]	−25.69	−25.689	−25.690
	$1^\circ < \theta < 179^\circ$	σ^{Born} [pb]	1.770	1.7696	1.7697
		δ [%]	−22.31	−22.313	−22.313
	20°	σ^{Born} [pb]	0.001869		0.0018688
		δ [%]	−41.57		−41.575
	90°	σ^{Born} [pb]	0.002334		0.0023340
		δ [%]	−41.98		−41.981
2000	160°	σ^{Born} [pb]	0.03094		0.030942
		δ [%]	−33.99		−33.994
	$20^\circ < \theta < 160^\circ$	σ^{Born} [pb]	0.04620	0.046201	0.046201
		δ [%]	−39.53	−39.529	−39.529
	$1^\circ < \theta < 179^\circ$	σ^{Born} [pb]	0.1170	0.1170	0.11697
		δ [%]	−30.84	−30.845	−30.845

observables and to impose experimental cuts. We have presented analytical expressions for the covariant amplitudes of the process and the helicity amplitudes for three different cross channels: Z boson production $f_1\bar{f}_1 \to Z\gamma$ and $f_1\gamma \to f_1 Z$, and for the decay $Z \to f_1\bar{f}_1\gamma$. To be assured of the correctness of our analytical results, we observe the independence of the form factors on the gauge parameters (all calculations were done in R_ξ gauge) and the validity of the Ward identity for the covariant amplitudes. We have compared our numerical results for these processes with other independent calculations. The Born level and the hard photon contributions of all three channels were checked against the CompHEP package, and we found a very good agreement except for the annihilation channel at high energies. For the channel $\gamma e^- \to Ze^-(\gamma)$, the comparison of the SANC EW NLO predictions with the results of [4, 26] has shown excellent agreement in a wide range of CMS energies and final electron scattering angles.

The results presented lay a base for subsequent extensions of calculations in the annihilation channel appropriate to the process $pp \to XZ\gamma$ at hadron colliders.

Acknowledgements. This work is partly supported by INTAS grant No. 03-51-4007 and by the EU grant mTkd-CT-2004-510126 in partnership with the CERN Physics Department and by the Polish Ministry of Scientific Research and Information Technology grant No. 620/E-77/6.PRUE/DIE 188/2005-2008 and by Russian Foundation for Basic Research grant No. 07-02-00932.

WvS is indebted to the directorate of the Dzhelepov Laboratory of Nuclear Problems, JINR, Dubna for the hospitality extended to him during September 2007.

References

1. R. Mertig, M. Bohm, A. Denner, Comput. Phys. Commun. **64**, 345 (1991)
2. T. Hahn, M. Perez-Victoria, Comput. Phys. Commun. **118**, 153 (1999) [hep-ph/9807565]
3. T. Hahn, Comput. Phys. Commun. **140**, 418 (2001) [hep-ph/0012260]
4. G. Belanger et al., Phys. Rep. **430**, 117 (2006) [hep-ph/0308080]

5. A. Andonov et al., Comput. Phys. Commun. **174**, 481 (2006) [hep-ph/0411186]
6. Dubna, http://sanc.jinr.ru
7. CERN, http://pcphsanc.cern.ch
8. D. Bardin, S. Bondarenko, L. Kalinovskaya, G. Nanava, L. Rumyantsev, Eur. Phys. J. C **52**, 83 (2007) [hep-ph/0702115]
9. D. Bardin et al., hep-ph/0506120
10. D0 Collaboration, V.M. Abazov et al., Phys. Lett. B **653**, 378 (2007) [0705.1550 [hep-ex]]
11. D0 Collaboration, V.M. Abazov et al., Phys. Rev. Lett. **95**, 051 802 (2005) [hep-ex/0502036]
12. CDF II Collaboration, D. Acosta et al., Phys. Rev. Lett. **94**, 041 803 (2005) [hep-ex/0410008]
13. U. Baur, D.L. Rainwater, Phys. Rev. D **62**, 113 011 (2000) [hep-ph/0008063]
14. S. Haywood et al., hep-ph/0003275
15. S. Atag, I. Sahin, Phys. Rev. D **70**, 053 014 (2004) [hep-ph/0408163]
16. R. Walsh, A.J. Ramalho, Phys. Rev. D **65**, 055 011 (2002)
17. E. Accomando, A. Denner, C. Meier, Eur. Phys. J. C **47**, 125 (2006) [hep-ph/0509234]
18. T.G. Rizzo, Phys. Rev. D **54**, 3057 (1996) [hep-ph/9602331]
19. S. Atag, I. Sahin, Phys. Rev. D **68**, 093 014 (2003) [hep-ph/0310047]
20. M.A. Perez, F. Ramirez-Zavaleta, Phys. Lett. B **609**, 68 (2005) [hep-ph/0410212]
21. B. Ananthanarayan, S.D. Rindani, R.K. Singh, A. Bartl, Phys. Lett. B **593**, 95 (2004) [hep-ph/0404106]
22. M. Capdequi Peyranere, Y. Loubatieres, M. Talon, Nuovo Cim. A **90**, 363 (1985)
23. F.A. Berends, G.J.H. Burgers, W.L. van Neerven, Phys. Lett. B **177**, 191 (1986)
24. M. Bohm, T. Sack, Z. Phys. C **35**, 119 (1987)
25. A. Denner, S. Dittmaier, hep-ph/9308360
26. A. Denner, S. Dittmaier, Nucl. Phys. B **398**, 265 (1993)
27. W. Hollik, C. Meier, Phys. Lett. B **590**, 69 (2004) [hep-ph/0402281]
28. G.P. Lepage, J. Comput. Phys. **27**, 192 (1978)